CrossMark

Influence of the May Southern annular mode on the South China Sea summer monsoon

Ting Liu[1] · Jianping Li[2,3] · YanJie Li[4] · Sen Zhao[5,6] · Fei Zheng[4] · Jiayu Zheng[1] ·
Zhixiong Yao[1]

Abstract The possible impact of the May Southern Hemisphere (SH) annular mode (SAM) on the following South China Sea (SCS) summer monsoon (SCSSM) is examined. A close inverse relationship between the two is revealed in the observations. The simultaneous South Pacific dipole (SPD), a dipole-like sea surface temperature anomaly pattern in the South Pacific, acts as the "oceanic bridge" to preserve the May SAM signal and prolong it into June–September. Observational evidence and numerical simulations both demonstrate that the SPD communicates its large thermal inertia signal to the atmosphere, regulating the Southern Pacific Subtropical Jet (SPSJ) variability over eastern Australia. Corresponding to the adjustment of circulation associated with the SPSJ is a prominent tripolar cross-Pacific teleconnection pattern stretching from the SH middle–high latitudes into the NH East Asia coastal region, referred to as the South–North Pacific (SNP) teleconnection pattern. Wave ray tracing analysis manifests that the SNP acts as the "atmospheric bridge" to propagate the related wave energy across the equator and into the Maritime Continent and SCS monsoon region, modulating the vertical motion and middle–lower tropospheric flows, and favoring the out-of-phase variation of the SCSSM. Therefore, the "coupled oceanic-atmospheric bridge" process and the related Rossby wave energy transmission are possible mechanisms for the significant influence of the May SAM on the variability of the following SCSSM. Therefore, the May SAM provides a fresh insight into the prediction of the SCSSM from the perspective of the SH high latitudes.

This paper is a contribution to the special issue on East Asian Climate under Global Warming: Understanding and Projection, consisting of papers from the East Asian Climate (EAC) community and the 13th EAC International Workshop in Beijing, China on 24–25 March 2016, and coordinated by Jianping Li, Huang-Hsiung Hsu, Wei-Chyung Wang, Kyung-Ja Ha, Tim Li, and Akio Kitoh.

✉ Jianping Li
  ljp@bnu.edu.cn

✉ YanJie Li
  lyj@mail.iap.ac.cn

1 State Key Laboratory of Satellite Ocean Environment Dynamics, Second Institute of Oceanography, Hangzhou, China

2 State Key Laboratory of Earth Surface Processes and Resource Ecology and College of Global Change and Earth System Science, Beijing Normal University, Beijing 100875, China

3 Laboratory for Regional Oceanography and Numerical Modeling, Qingdao National Laboratory for Marine Science and Technology, Qingdao 266237, China

4 State Key Laboratory of Numerical Modeling for Atmospheric Sciences and Geophysical Fluid Dynamics, Institute of Atmospheric Physics, Chinese Academy of Sciences, Beijing, China

5 School of Ocean and Earth Science and Technology, University of Hawaii at Mānoa, Honolulu, HI, USA

6 Key Laboratory of Meteorological Disaster of Ministry of Education, and College of Atmospheric Science, Nanjing University of Information Science and Technology, Nanjing, China

1 Introduction

The Southern Hemisphere (SH) annular mode (SAM) is the dominant mode of large-scale atmospheric activity in the middle and high latitudes of the SH (Gong and Wang 1998; Thompson and Wallace 2000; Li and Wang 2003), covering an extensive latitudinal band in the SH extra-tropics and with a global scale in the meridional direction. The large scale spatial characteristic of the SAM not only guarantees that it plays a pivotal role in SH climate variability (Thompson and Solomon 2002; Gillett et al. 2006; Marshall and Connolley 2006; Fogt et al. 2012), but also means that the climatic influence of the SAM is not just confined to the SH. Previous research has provided some evidence that a preceding anomalous SAM signal has the potential to regulate climate in the Northern Hemisphere (NH), especially for the NH monsoons. Specifically, Nan and Li (2003) first revealed that the precursor spring SAM could modulate the following East Asian summer monsoon (EASM) precipitation by virtue of the "coupled oceanic-atmospheric bridge" process (Nan and Li 2005a, b; Nan et al. 2009; Li 2016). Analogously, the boreal autumn SAM affects the following winter monsoon in China (Wu et al. 2009) and precipitation over East Asia (Liu et al. 2015, 2016; Wu et al. 2015). The boreal winter SAM also exhibits an out-of-phase relationship with spring precipitation variability over South China (Zheng and Li 2012; Zheng et al. 2015a). As well as being related to the East Asian monsoon region, the preceding SAM is closely related to the West African Summer Monsoon (Sun et al. 2010), North American Summer Monsoon (Sun 2010) and Indian Summer Monsoon (Viswambharan and Mohanakumar 2012; Prabhu et al. 2015; Dou et al. 2016).

Essentially, the cross-seasonal and cross-equatorial impacts of the SAM mentioned above are realized due to various "coupled oceanic-atmospheric bridge" processes. In simple terms, the sea surface temperature (SST) acts as the "oceanic bridge" to preserve the anomalous SAM information via oceanic dynamic and thermodynamic processes, and persists for a long period due to the large thermal inertia of the oceans. The thermal communication of the SAM-related SST then drives following atmospheric responses that link the NH climate and the SAM-related SST (Li 2016). Therefore, such cross-seasonal and cross-equatorial influences of the preceding SAM on the climate variability in the NH monsoon regions provide fresh clues for the seasonal prediction of the NH monsoons.

The South China Sea (SCS) monsoon region (0°–25°N, 100°–125°E) is the core area of the Asian–Australian monsoon, and is the hub connecting four monsoon subsystems (Murakami et al. 1986; Wang et al. 2009; Li and Hu 2011): the Australian monsoon, the Indian monsoon, the western North Pacific (WNP) monsoon, and the East Asian monsoon.

The onset of the SCS summer monsoon (SCSSM) marks the beginning of the rainy season in eastern China (Tao and Chen 1987; Murakami and Matsumoto 1994; Lau and Yang 1997; Wu and Wang 2000, 2001; Ding et al. 2004; Chen et al. 2006; Feng and Li 2009; Li and Hu 2011). The SCSSM activity is closely related to the climate variability over and beyond the adjacent regions (Ding 1992; Zhu et al. 2003; Lestari 2010). The atmospheric teleconnections [such as the Pacific–Japan teleconnection (Nitta 1987); East Asia-Pacific teleconnection (Huang and Li 1987, 1988; Huang 2004); East Asia–Pacific–Northern American teleconnection (Li and Zhang 1999; Ding et al. 2004); Circum-Pacific teleconnection (Kawamura et al. 1996; Fukutomi and Yasunari 2002; Wang et al. 2009); Indian Ocean–East Asia–Pacific teleconnection (Li et al. 2013a, c)] excited by convection over the northern SCS during the prevailing period of the SCSSM can transport the influence of the SCSSM to East Asia and North America and even over large areas of the NH.

In addition, the SST anomaly (SSTA) in the Southern Ocean may be seen as an indicator for the SCSSM onset (Lin et al. 2013), but the physical mechanisms of this cross-equatorial connection are far from systematically demonstrated. Meanwhile the SSTA in the Southern Ocean are interwoven with the SAM variability (Wu et al. 2009; Zheng and Li 2012; Liu et al. 2015, 2016; Zheng et al. 2015a, b). Hence, considering the large spatial scale of the SAM, its influence on the NH monsoon may extend beyond the aforementioned monsoon regions. Therefore, it is necessary to understand the SCSSM variability, which may provide valuable information for the EASM, starting from the preceding SAM signal.

The principal purpose of this work is to probe the potential influence of the preceding May SAM on the following June–September (JJAS) SCSSM variability, and examine the possible underlying physical mechanisms. This paper is organized as follows. Details of the data and methods are discussed in Sect. 2. Section 3 explores the relationship between the May SAM and the JJAS SCSSM, and physical mechanisms are proposed to interpret the role of the "coupled oceanic-atmospheric bridge" process in prolonging the SAM signal and transmitting its influence cross-equatorially to the SCSSM region. Numerical experiments and wave ray tracing techniques are employed to provide further evidence for the physical mechanism in this section. Finally, the conclusions and discussions of some outstanding issues are presented in Sect. 4.

2 Data, methodology and model

2.1 Data and methods

The main datasets employed in the present analysis are: (1) meteorological elements from the European Centre

for Medium-Range Weather Forecasts (ECMWF) reanalysis interim (ERA-Interim) dataset (Berrisford et al. 2011); (2) SST data used are extracted from the NOAA Extended Reconstructed Sea Surface Temperature version 3 (ERSST V3; Smith et al. 2008). We also employ the National Centers for Environmental Prediction–National Center for Atmospheric Research (NCEP/NCAR; Kalnay et al. 1996) reanalysis dataset and the Hadley Centre Sea Ice and Sea Surface Temperature dataset (HadISST; Rayner et al. 2003) to verify the results. The results are not sensitive to choice of product, giving us the confidence that our conclusion are robust. Data coverage in this study is focused on the period from 1979 to 2015, after the introduction of satellite records to ensure the reliability of SH data.

The SAM index (SAMI) modified by Nan and Li (2003) (see also Li 2016, http://ljp.lasg.ac.cn/dct/page/65609) is employed to represent the variability of the SAM. This SAMI is significant correlated with SAMI defined by Marshall (2003), with correlation coefficient of 0.86 in May for the period 1979–2005. Similar results can be reached by making the same analysis with different versions of SAMI, indicating that the conclusion here is insensitive to the choice of SAMI. Hereafter, SAMI refers to the definition given by Nan and Li (2003). The variability of the El Niño-Southern Oscillation (ENSO) is described by the Niño 3.4 index (http://www.cpc.ncep.noaa.gov/-data/indices/3mth.nino34.81-10.ascii.txt).

The SCSSM index (SCSSMI) used hereafter is derived from the unified Dynamic Normalized Seasonality (DNS) index defined by Li and Zeng (2000, 2002, 2003, 2005 http://ljp.gcess.cn/dct/page/65578). The DNS index is based on seasonal alternation in wind direction over monsoon regions, and can be widely practiced to depict the seasonal cycle and inter-annual variability of the different monsoons (Li et al. 2010; Zhu et al. 2012; Shi et al. 2014; Zheng et al. 2014b; An et al. 2015; Feng et al. 2015). For a given pressure level, the DNS index in the mth month of the nth year on the grid point (i, j) is given by

$$\delta_{nm} = \frac{\left\| \overrightarrow{V_1} - \overrightarrow{V}_{nm} \right\|}{\overrightarrow{V}} - 2,$$

where $\overrightarrow{V_1}$ is the January climatological wind vector, $\overrightarrow{V}$ is the mean of the January and July climatological wind vectors, and $\overrightarrow{V}_{nm}$ is the monthly wind vector for the mth month of the nth year. Then the SCSSMI is defined as the seasonal (JJAS) areal mean DNS over the SCS domain (0°–25°N, 100°–125°E) at 925 hPa.

To exclude the impact of the ENSO signal on the linkage between the May SAM and the following SCSSM, the partial correlation is employed throughout the paper. The two-tailed Student's t test using the effective number of

degrees of freedom (N^{eff}) is applied to ascertain the statistical significance of the correlation coefficients between two auto-correlated time series, such as SST in this paper. The N^{eff} is based on Li et al. (2013b) and is given as:

$$\frac{1}{N^{eff}} = \frac{1}{N} + \frac{2}{N} \sum_{i=1}^{N} \frac{N-i}{N} \rho_{XX}(i) \rho_{YY}(i),$$

where N is the sample size, and $\rho_{XX}(i)$ and $\rho_{YY}(i)$ are the autocorrelations of two sampled time series X and Y at time lag i, respectively.

2.2 Numerical model and tools for analyzing Rossby wave propagation

The NCAR Community Atmosphere Model version 5 (CAM5) is employed to gain more dynamic insight into the atmospheric response to the SAM-related SST forcing. CAM5 is the atmospheric component of the Community Earth System Model (CESM 1.0.4.). The finite-volume dynamical core of CAM5 has 42-wave triangular spectral truncation (T42) and 30 vertical levels from the surface up to 2.25 hPa.

Rossby wave ray tracing is a theoretical tool for detecting energy dispersion of stationary Rossby wave (Hoskins and Karoly 1981; Li and Li 2012; Li et al. 2015; Zhao et al. 2015), and is applied widely in climate research involving teleconnection mechanisms (Xu et al. 2013; Sun et al. 2015, 2016; Wu et al. 2016; Zheng et al. 2016). The wave ray trajectory can be calculated from the dispersion relation of the barotropic nondivergent vorticity equation on a time-mean slowly varying basic state. Here we employ the stationary Rossby wave ray method developed by Li et al. (2015) and Zhao et al. (2015) to delineate the propagation behavior of wave energy associated with the SAM-related basic flow.

3 Results

3.1 Relationship between the May SAM and the SCSSM

Figure 1a presents the lead-lag correlation between the monthly SAM index (SAMI) and the JJAS SCSSM index (SCSSMI). The strongest negative correlation (blue solid line, $r = -0.37$, significant at the 95% confidence level) occurs with the SAM leading SCSSM by 1 month. This implies that a positive May SAM is often accompanied by a weakened SCSSM. And the May SAM contributes up to 14% of the total variance of the JJAS SCSSM. This relationship between the May SAM and the following SCSSM
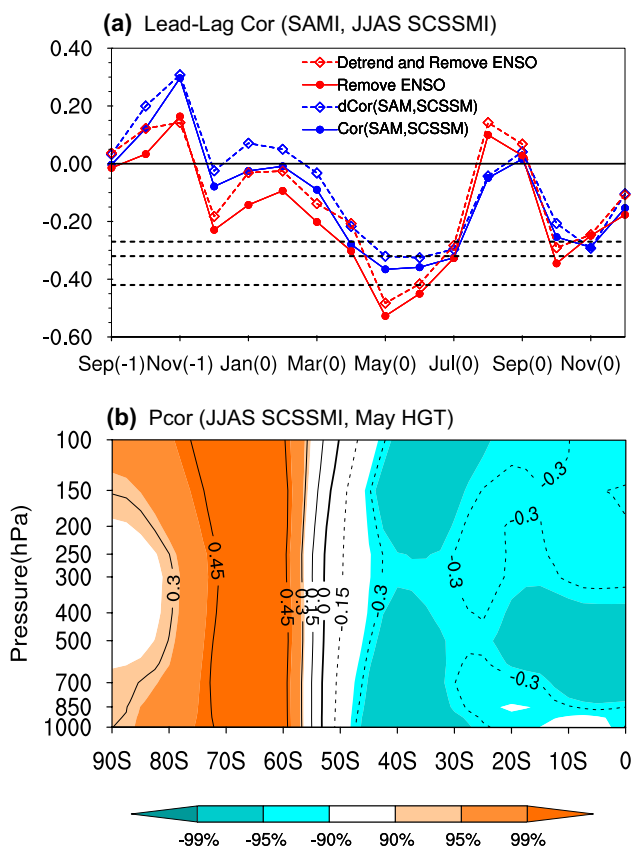
Fig. 1 **a** Lead-lag correlation between the monthly SAM index and JJAS SCSSM index. The *blue and red solid lines* indicate the result before and after removing the ENSO signal, respectively, and the *blue and red dashed lines* are the corresponding results with the trend removed. The *black dashed lines* indicate the Student's *t* test with 90, 95 and 99% level, respectively. **b** Partial correlation map of the May zonal mean geopotential height based on the JJSA SCSSM index after removing the ENSO signal. Correlation coefficients passing the Student's *t* test with 90% level are *shaded*

(blue dashed line, $r = -0.33$, significant at the 95% confidence level) remains significant for the detrended time series. In addition, the preceding winter (December–January, DJF) ENSO have the potential to modulate the following SCSSM variability (Wang et al. 2009), with the correlation coefficient of -0.37 (significant at the 95% confidence level). And the DJF ENSO also contributes to the May SAM variability (Ding et al. 2012, 2015), with the correlation coefficient of -0.28 (significant at the 90% confidence level). This indicates that the relationship between the May SAM and the JJAS SCSSM may be influenced by the DJF ENSO. Therefore, the partial correlation analysis is further applied to validate the linkage between the May SAM and the JJAS SCSSM with the DJF ENSO signal removed. Their correlation is strengthened considerably, giving a stronger negative correlation coefficient of -0.53 (red solid line, significant at the 99% confidence level). This suggests that the May SAM maybe a more important

factor modulating the SCSSM variability in the year without the influence of the ENSO. Furthermore, the result with both trend and ENSO signal removed is -0.48 (red dashed line, significant at the 99% confidence level), indicating that the inverse relationship between the May SAM and the following SCSSM is statistically robust. The correlation analysis suggests that the May SAM is a potential regulator of the following SCSSM activity, and further evidence will be shown in the discussion of the physic mechanism below.

In addition, Fig. 1b displays the correlation map of the preceding May zonal mean geopotential height against the JJAS SCSSMI after removing the ENSO signal. The outstanding feature is a typical negative SAM phase with an equivalent barotropic dipole-like pattern in the SH extratropical troposphere with opposite centers of geopotential height anomalies located near 40°S and 70°S. This further implies that prior to a strengthening SCSSM, a negative SAM exists over the whole troposphere. In brief, the above discussion from the perspectives of May SAM and SCSSM both indicate that the relationship between the May SAM and the following SCSSM is robust. So what is the physical mechanism responsible for this relationship? We will attempt to answer this question.

3.2 SST anomalies associated with the May SAM and SCSSM

It is generally recognized that the persistence of an atmospheric signal itself, such as the SAM, is limited. However, the vast thermal inertia of the ocean deriving from its heat storage capacity means that the signal of the SAM-induced SSTA can be communicated into the overlaying atmosphere, and making it possible to "prolong" the influence of the SAM on the remote climate (Nan and Li 2003, 2005a, b; Nan et al. 2009; Wu et al. 2009, 2015; Zheng and Li 2012; Zheng et al. 2014a, 2015a, b; Liu et al. 2015, 2016; Li 2016).

Accompanied with the SAM anomalies, a notable dipole pattern of surface zonal wind anomalies persists from the May to the boreal summer (Fig. 2). The positive SAM is usually associated with the strengthen westerlies in the high-latitudes and weaken westerlies in the mid-latitudes over South Pacific Ocean. High (low) wind speed can both increase (decrease) the ocean heat release at the atmosphere–ocean interface and induce the equatorward (poleward) Ekman transport of cold (warm) water (Gupta and England 2006). Through the above dynamic and thermodynamic processes, the surface wind anomalies associated with May SAM can induce the SSTA. Figure 3 presents SSTA patterns associated with the May SAM both for May and the following JJAS. During the positive May SAM cases, a noteworthy meridional dipole-like SSTA pattern in the South Pacific Ocean with warmer SSTA in the
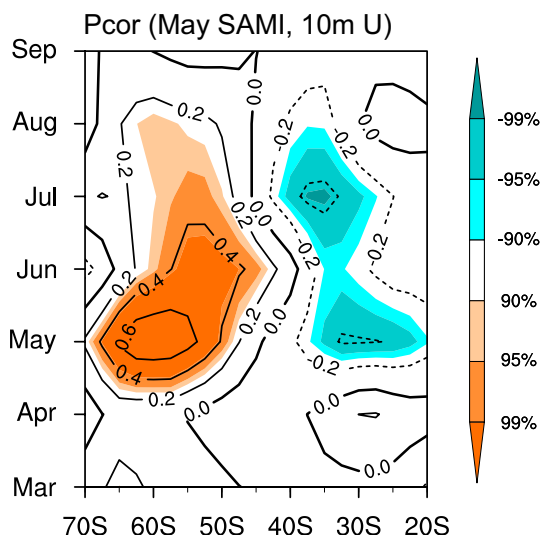
Fig. 2 The partial lead-lag correlation coefficients between the May SAMI and the 10 m zonal wind anomalies averaged over the South Pacific Ocean region (160–240°E) the from March to September after removing the ENSO signal. Correlation coefficients passing the Student's *t* test with 90% level are *shaded*

Fig. 3 The partial correlation maps of **a** May SST and **b** JJAS SST anomalies against the May SAM index after removing the ENSO signal. Correlation coefficients passing the Student's *t* test with 90% level are stippled

mid-latitudes and colder SSTA in the high-latitudes prevails from May (Fig. 3a) to JJAS (Fig. 3b).

To quantitatively portray this dipole-like SSTA pattern, a Southern Pacific SST Dipole (SPD) index (SPDI) is defined as the difference in the standardized regional zonal-average SSTA between 32°S and 56°S in the Southern Pacific Ocean (160°E–240°E). These two latitudes are selected because their regional zonal-average SSTA have the greatest negative correlated here. In fact, the SPD pattern SSTA is reflected in the leading mode of the SST variability in the South Pacific Ocean as referenced by Terray (2011) and Saurral et al. (2017). While the variability of the SPD is relatively weaker in May (Fig. 4a), however, the variability of the SAM began strengthening in the May (Fig. 4b). In the same month May, the correlation between the SAM and the SPD begins strengthen (Fig. 4c). This also implies that the May SAM have the potential to regulate the May SPD variability via the related dynamic and thermodynamic processes.

Meanwhile, the SPDI exhibits co-variability with the May SAMI from May into JJAS with correlation coefficients of 0.49 and 0.47 (significant at the 99% confidence level), respectively. The correlations between the May SAMI and SPDI in May and JJAS are still robust after removing ENSO, with the correlation coefficients of 0.43 and 0.42 (significant at the 99% confidence level), respectively. The auto-correlation analysis of the May SPDI reveals that the May SPD signal can maintain 5 months (Fig. 4d), and the lag correlation between the May SPDI and JJAS SPDI is 0.88 (significant at the 99% confidence
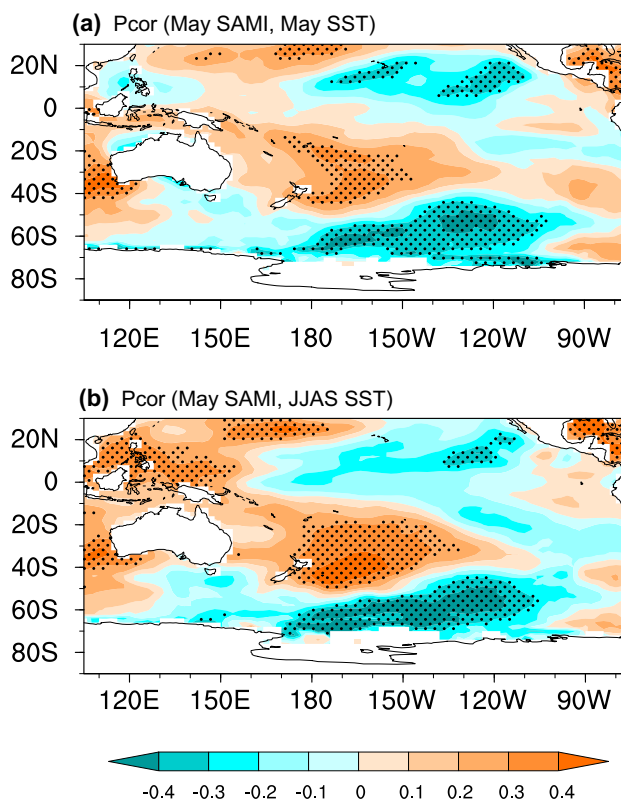
level using the effective numbers of degrees of freedom). This further indicates that the May SAM signal can be impressed on the SPD and prolonged into JJAS via the huge thermal inertia of the ocean.

Furthermore, the SCSSMI is also highly negatively correlated with the SPDI from May into JJAS with correlation coefficients of −0.32 and −0.49 (significant at the 95 and 99% confidence level), respectively. This is consistent with the inverse relationship between the May SAM and the following SCSSM. Moreover, the partial correlation coefficients between the May SAM and the following SCSSM after removing the May and JJAS SPDI are −0.26 and −0.19, respectively. In contrast to the raw correlation (−0.37), the relationship between the two becomes weaker and non-significant after eliminating the SPD signal. Combining the result with the significant correlation between the SPDI and the May SAM and the following SCSSM, and the high lag correlation of the SPDI in May and JJAS, implies that the memory of the SST in the Southern Pacific Ocean acts as a crucial bridge connecting the May SAM and the following SCSSM. We now focus on how such SPD SSTA

Fig. 4 **a** The standard deviations of monthly SPDI. **b** The standard deviations of monthly SAMI. **c** The partial correlation coefficients between monthly SAMI and SPDI after removing the trend and ENSO signal; **d** The partial auto-correlation of May SPDI after removing the trend and ENSO signal

communicates with the overlying atmospheric circulation and enable the cross-equatorial influence on the SCSSM.

3.3 Influence of the SPD on the atmospheric circulation

The SAM involves fluctuations of the westerly jet via wave-mean interaction (Hoskins and Karoly 1981; Hartmann and Lo 1998; Limpasuvan and Hartmann 1999, 2000; Thompson and Wallace 2000; Lorenz and Hartmann 2001; Li and Wang 2003; Marshall and Connolley 2006; Frierson et al. 2007; Chen et al. 2010; Zheng et al. 2015a). In general, SAM-related dipole-like SSTA can induce anomalous eddy activity by altering the regional baroclinicity. The westerly jet then adjusts to balance the related variation of eddy momentum. We therefore investigate the JJAS zonal wind variability averaged over the Pacific Ocean (160°–240°E) associated with the JJAS SPD forcing (Fig. 5a). The distribution of zonal wind anomalies extends throughout the tropopause as alternating positive and negative correlation pattern extending from the SH mid-latitudes to the NH subtropics. The negative anomalies of zonal wind at 20°–30°S

correspond to a weakened Southern Pacific Subtropical Jet (SPSJ, at 200 hPa) over eastern Australia. The activity of this subtropical jet can also induce an adjustment of the circulation manifested as anomalous easterlies over the tropics and anomalous westerlies over 20°N, indicating that the cross-equatorial propagation of the SPD signal may spread into the SCS monsoon region.

To quantitatively depict the variability of this SPSJ, the standardized maximum 200 hPa zonal wind over the Southern Pacific Ocean region is defined as the SPSJ index (SPSJI). Figure 5b presents time series of the JJAS SPSJI (red line) and SPDI (blue line). Both are dominated by the interannual variability and the SPSJI is significantly inversely correlated with the SPDI, with a correlation coefficient of −0.51 ($r = −0.52$ after removing the ENSO signal), which is significant at the 99% confidence level. Meanwhile, the SPSJI also exhibits high co-variability with the SCSSMI with a correlation coefficient of 0.55 ($r = 0.6$ after removing the ENSO signal), which is significant at the 99% confidence level. This result further indicates that the positive SPD can induce the weakened SPSJ, and the
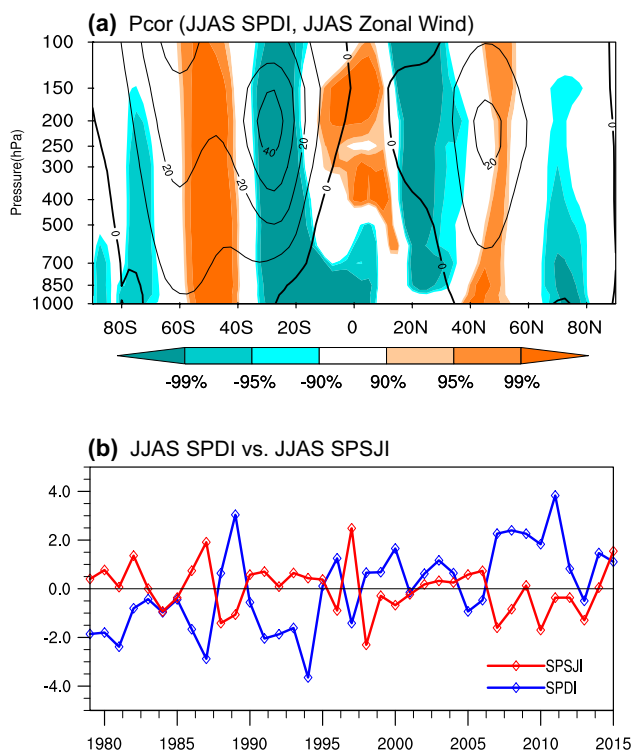
(a) Pcor (JJAS SPDI, JJAS Zonal Wind)

(b) JJAS SPDI vs. JJAS SPSJI

Fig. 5 **a** The partial correlation map of the JJAS zonal wind averaged over the Pacific Ocean region (160–240°E) against the JJAS SPD index after removing the ENSO signal. Correlation coefficients passing the Student's *t* test with 90% level are *shaded*. Contours indicate the JJAS climatological zonal wind averaged over the South Pacific Ocean region (160–240°E). **b** The time series of JJAS SPD index (*blue*) and SPSJ index (*red*) for 1979–2015

Zonal wind in CAM5

Fig. 6 Simulated composite difference of the response of the JJAS zonal wind averaged over the Pacific Ocean region (160–240°E) to forcing by positive and negative JJAS SPD pattern SSTA. *Contours* indicate the JJAS climatological zonal wind averaged over the Pacific Ocean region (160–240°E)

influence of the related circulation adjustment can also spread into the NH, corresponding to a weakened SCSSM.

We also conduct sensitivity experiments with the CAM5 numerical model to gain further dynamical insights into the influence of the SPD on the SPSJ. The control run is forced by a climatological monthly varying SST, sea-ice concentration, ozone concentration and carbon dioxide, repeated annually. Composite JJAS SSTA south of 30°S in high (SPDI > 1.0) and low (SPDI < −1.0) SPD cases are superimposed on the climatology to driven the positive and negative sensitivity experiments. All the numerical integrations are run for 33 years, and the results of the last 25 years are employed for the comparison experiment to exclude the model initialization shock. The experiments approximately capture the observed distribution of the zonal wind averaged over the Pacific Ocean (160°–240°E), corresponding to a weaker SPSJ and positive-to-negative zonal wind anomalies extending from the SH mid-latitudes to the NH subtropics in response to SPD forcing (Fig. 6). Despite the crudeness of the AGCM simulations, which lack air–sea feedback, the overall consistence of the model performance with observations supports the idea that the SPD has the
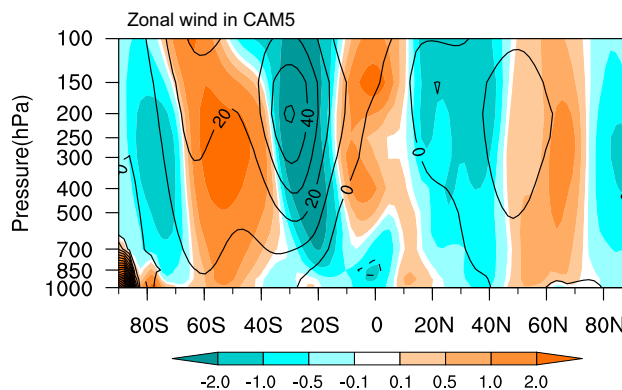
potential to regulate the SPSJ activities and that the influence of the related circulation adjustment may propagate into the NH to impact the SCSSM.

In fact, the distribution of zonal wind anomalies over the Pacific Ocean corresponds to the anticyclonic-to-cyclonic shear in the flow field. Figure 7a presents the correlation map of the 200 hPa stream function with the JJAS SPSJI. There is a notable tripole ("− + −") of large-scale anomalies across the Pacific Ocean with centers in the middle latitudes of the Southern Pacific, tropical central and west Pacific, and NH subtropical Pacific, constituting a teleconnection wave train stretching from the SH middle-high latitudes into the NH East Asian coastal region. For convenience, such a tripolar teleconnection wave pattern is referred to as the South–North Pacific teleconnection pattern (SNP), and the SNP index is defined as.

$$SNPI = \phi_B - \frac{1}{2}(\phi_A + \phi_C),$$

where ϕ_A, ϕ_B, ϕ_C are the normalized area-averaged stream function anomalies in the green box A (5°–30°N, 125°–240°E), box B (2.5°–22.5°S, 100°–210°E), and box C (25°–50°S, 180°–280°E), respectively. This index is highly correlated with the SPSJI with a correlation coefficient is −0.80 (significant at the 99% confidence level), indicating that the influence of the variation of the SPSJ is not limit to the local region, but induces the adjustment of circulation and the cross-equatorial SNP.

A similar tripolar teleconnection wave train can also be identified in the correlation analysis of the JJAS 200 hPa stream function with SPDI (Fig. 7b), SCSSMI (Fig. 7c) and May SAM (Fig. 7d). Here however the phase of the SPD-associated and SAM-associated SNPs are opposite to the phase of the SPSJI-associated SNP, while the
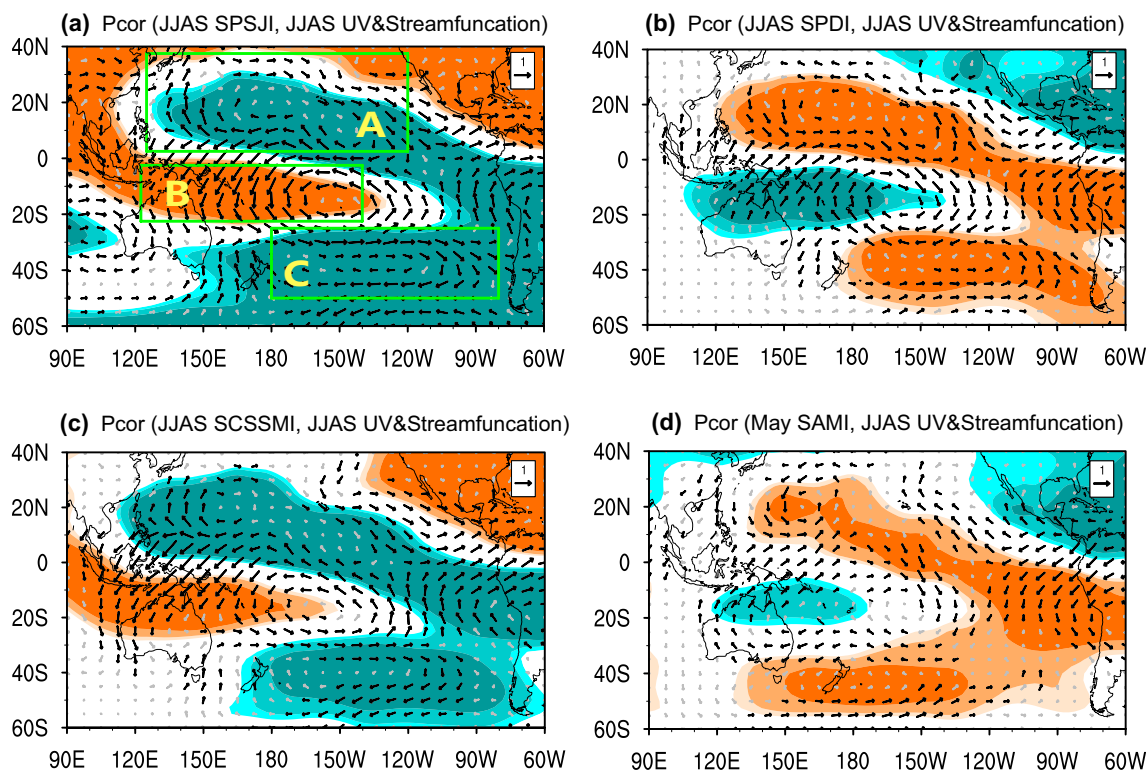
Fig. 7 The partial correlation maps of the 200 hPa JJAS stream function (*shading*) and horizontal wind (*vectors*) against the **a** JJAS SPSJ index, **b** JJAS SPD index, **c** JJAS SCSSM index, and **d** May SAM index after removing the ENSO signal. *Shading and black vectors* indicate the correlation coefficients passing the Student's *t* test with 90% level

SCSSM-associated SNP is in phase of the SPSJI-associated SNP. These results consistent with the negative correlation between the SPSJ and SPD (SAM), and positive correlation between the SPSJ and SCSSMI. The May SAM, JJAS SPD, JJAS SPSJ and SCSSM are all closely correlated with the SNP, with correlation coefficients are 0.45, 0.62, −0.80 and −0.64 (both significant at 99% confidence level), respectively. After removing the ENSO signal, the corresponding correlation coefficients are 0.44, 0.62, −0.80 and −0.72 (both significant at 99% confidence level), respectively. Meanwhile, the correlation coefficients of the May SAMI, JJAS SPDI, and JJAS SPSJI against SCSSMI significantly weakens from −0.37 (−0.49, 0.55) to −0.12 (−0.19, 0.09) after removing the SNP signal. The above analysis implies that the SNP, which is related to the SPSJ-induced circulation adjustment, is the crucial atmospheric link in the connection between the SAM or SPD and the SCSSM.

To provide further dynamical insight into the SNP teleconnection pattern, the propagation of wave energy behavior is investigated with the wave ray tracing techniques mentioned in Sect. 2. Figure 8 displays the wave ray paths from several initial points located at the southern tip of the SNP teleconnection. The choice of the initial zonal wavenumbers is in accordance with the largest zonal wavelength of the SPN. The May SAM-regressed

200 hPa JJAS climatology mean flow is employed as the background state for calculating the wave ray trajectories to probe the influence of the May SAM-related basic flow on JJAS wave propagation behavior. The wave ray trajectories mainly travel northward into the SH subtropical region and then turn toward the northwest, following the path the pathway of the SNP teleconnection. The related wave energy
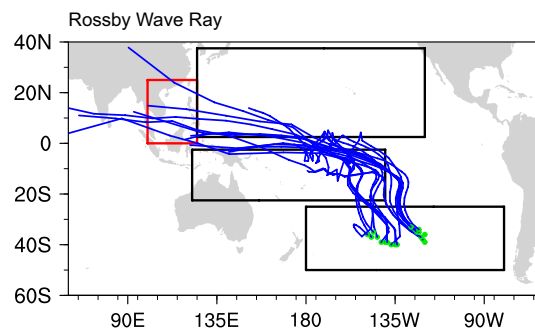

Fig. 8 Rossby wave ray trajectories (*blue lines*) starting from the southern source area (*green dots*) of the SNP teleconnection. The climatological mean of May SAM-regressed 200 hPa JJAS wind serves as the background field for calculating the wave ray trajectory. The *black boxes* indicate the location of the SNP teleconnection as shown by the *green boxes* in Fig. 7. The *red box* indicates the SCS monsoon region

can still reach the Maritime Continent and SCS monsoon region. This is further proof that the May SAM is a crucial precursor of the following SCSSM variability, and the associated wave energy propagation serves as a "bridge" to convey the impact of the May SAM on the SCSSM. We will next explore how the SNP affects the SCSSM.

3.4 Influence of the SNP on the regional circulation in the SCS

The anticyclonic-to-cyclonic shear related to the SNP in the upper troposphere certainly affect the horizontal convergence, and then transfers this influence into the vertical motion and lower troposphere atmospheric circulation.

Figure 9a, b present the height–latitude sections of the correlation of JJAS vertical velocity and meridional wind anomalies against the SNP in the SCS monsoon region, respectively. In the positive SNP case, there is notable anomalous clockwise vertical circulation with anomalous downward motion (Fig. 9a, red shading) over 10–20°N, and lower-tropospheric northerlies (Fig. 9b, green shading) over 0–10°N, weakening the updraft branch and meridional component of the SCSSM circulation (vectors), respectively. This is opposite of the situation of the strong SCSSM years, when there is significant anticlockwise vertical circulation with anomalous upward motion (Fig. 9c, green shading) over 10–20°N, and lower-tropospheric southerlies (Fig. 9d, red shading) over 0–10°N. Thus the
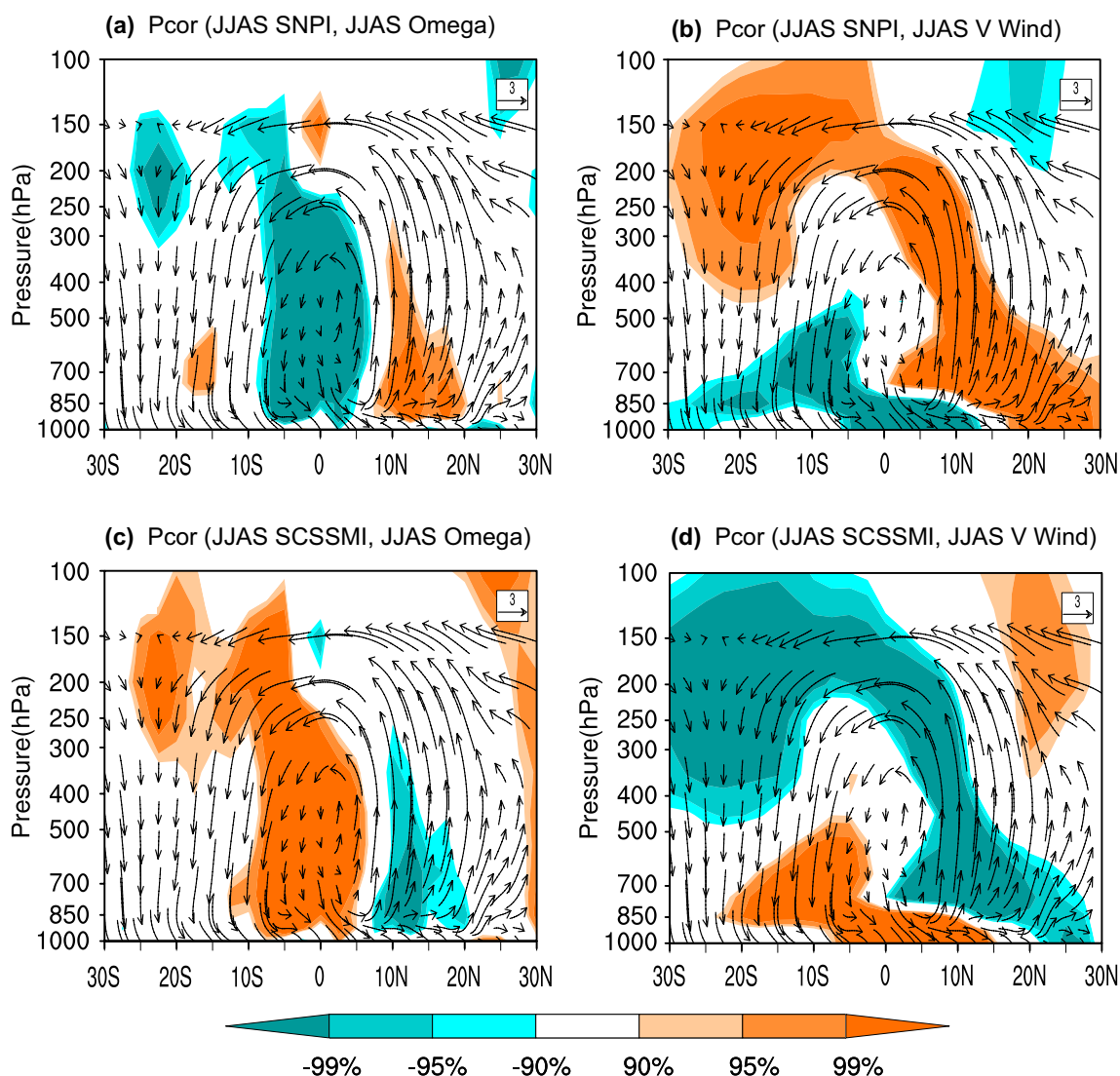

Fig. 9 The partial correlation maps of the JJAS **a** vertical velocity and **b** meridional wind (*shading*) averaged over the SCS monsoon region (100–125°E) against the JJAS SNP index after removing the ENSO signal. **c, d** same as **a, b**, but against the SCSSM index. *Vec-tors* indicate the climatological mean meridional circulation over the SCS monsoon region (100–125°E). Correlation coefficients passing the Student's *t* test with 90% level are *shaded*

cross-equatorial tripolar SNP has the potential to modulate the monsoon circulation in the SCS monsoon region, inducing the out of phase variation of the SCSSM.

The variation of monsoon circulation associated with the SNP can promote the influence of SNP to the lower troposphere, and lead to corresponding variations of horizontal circulation. Figure 10 presents the anomalous circulations associated with the SCSSM (Fig. 10a, b) and SNP (Fig. 10c, d). In enhanced SCSSM year, there is an anomalous cyclonic circulation cover the SH middle and high latitude, and northerly winds anomalies from the NH middle–high latitudes successively meet the westerly wind from the Indian Ocean and the cross-equatorial flow from Australia in the SCS monsoon region (red box in Fig. 10a). These anomalous flows can extend directly into the middle troposphere (500 hPa, Fig. 10b). When the SNP is in its positive phase, a significant anticyclonic circulation locates in the SH middle and high latitude, and the corresponding anomalous easterly flow from the Pacific and cross-equatorial easterly flows originating in the NH prevail in the SCS monsoon region in the middle (850 hPa, Fig. 9c) and low troposphere (500 hPa, Fig. 9d). The flow in these two branches can weaken the prevailing flow of the SCSSM and lead to a weak SCSSM.

In conclusion, it can be inferred from the above discussion that the May SAM signal is imprinted on the simultaneous SPD and prolonged into JJAS via the huge thermal inertia of the ocean. The SPD thermal forcing induces the variation of the SPSJ accompanying the adjustment of circulation. The SNP wave train pattern, which can stretch to the East Asian coast, is then often associated with this atmospheric circulation variability and modulates the vertical movement and circulation in the SCS monsoon region by altering the horizontal convergence.

4 Summary and discussion

The SCSSM bridges the communication gap for the four monsoon subsystems in the Asian–Australian monsoon. The variations of the SCSSM are linked with climate variability in East Asian, North America and even over a wider extend in the NH. Much effort has been devoted to investigating the influence of tropical factors on the SCSSM. However, little attention has been directed to exploring possible high-latitude influence on SCSSM variability, especially from the SH perspective. In this paper, we investigate the possible influence of the May SAM on the following SCSSM, and observe a close inverse relationship between the May SAM and the following SCSSM (Fig. 1). Enhancing our understanding of the physical mechanisms involved in such a remote impact of the SAM is essential not only for broadening our view of the cross-equatorial climate impact of SAM, but also for providing a fresh insight into the predictions of the SCSSM.
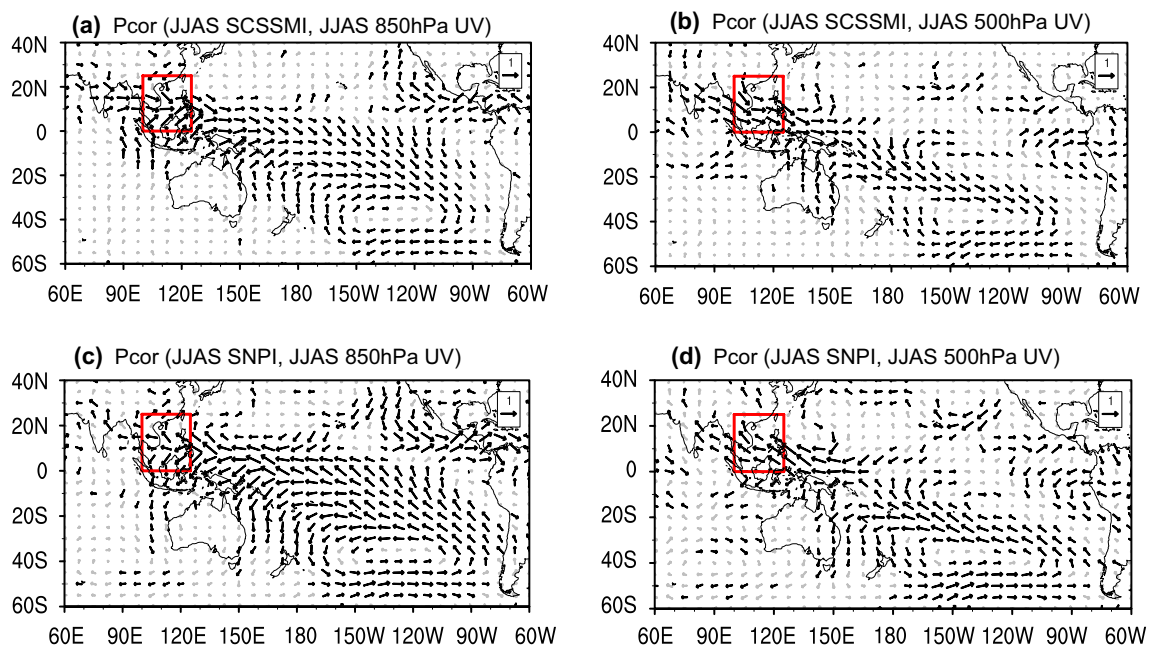

Fig. 10 The partial correlation maps of the JJAS horizontal wind at **a** 850 hPa, **b** 500 hPa, against the JJAS SCSSM index. **c, d** as for **a, b**, but against the JJAS SNP index after removing the ENSO signal.

Black vectors are values passing the Student's *t* test with 90% confidence level. The *red box* marks the SCS monsoon region (0–25°N, 100–125°E)

Given the limited persistence of the SAM signal, and the fact that the predictability of the SAM signal originates from coupling mechanisms with the underlying ocean forcing, we examine the SSTA associated with the May SAM and JJAS SCSSM (Figs. 2, 3, 4). The results suggest that the SPD SSTA in the South Pacific plays an "oceanic bridge" role linking the May SAM and the following SCSSM. The huge heat storage capacity of the ocean, allows the SPD to serve as a "memorizer" to preserve the information of the May SAM and prolong it into JJAS. The SPD can then communicates the signal deriving from its large thermal inertia to the atmosphere via wave-mean interaction. Both observational (Fig. 5) and model simulating results (Fig. 6) indicate that the SPD can regulate the variation of the SPSJ (at 200 hPa) over eastern Australia, giving also alternating anticyclonic and cyclonic shear over the Pacific Ocean. These upper-level divergence/convergence anomalies can induce anomalous wave activity, and excite the SNP wave train (Fig. 7). Results from wave ray tracing analysis demonstrate that the wave energy propagation associated with the SNP can cross the equator and reach into the Maritime Continent and SCS monsoon region (Fig. 8) and then modulate the monsoon circulation (Fig. 9) and horizontal atmospheric circulation in the middle and lower troposphere (Fig. 10) in the SCS monsoon region via adjustment of the horizontal convergence. Therefore, the responses of the SPSJ and SNP to the SPD serve as an "atmospheric bridge" to promote the impact of the SPD into the SCS monsoon region. Thus, this study provides a dynamical insight into the SAM–SCSSM relationship. A positive SAM often favors a positive SPD. The coordinated variation of the SPD may induce a weaker SPSJ and positive SNP wave train with anomalous downward motion and lower tropospheric northerly winds over the SCS monsoon region, which oppose the direction of the prevailing flow of the SCSSM, and thus weaken the SCSSM. The situation tends to be reversed with a negative SPD. In brief, it is the "coupled oceanic-atmospheric bridge" process and the related wave energy propagation in the South Pacific Ocean that conveys the influence of the May SAM onto the following JJAS SCSSM variability, as shown in the Fig. 11.

Our analysis indicates that the May SAM provides a supernumerary predictor for the SCSSM. Therefore, future research should focus on establishing a physically based empirical model for studying SCSSM prediction, combined with SAM and other predictors that also regulate the SCSSM. Meanwhile, it is vital to assess the capability of the existing coupled models to reproduce the SAM–SCSSM connection and to identify the possible factors constraining model performance. Proceeding from the above two aspects, we can expect to improve the prediction skills of the SCSSM. Moreover, the SNP wave pattern is a
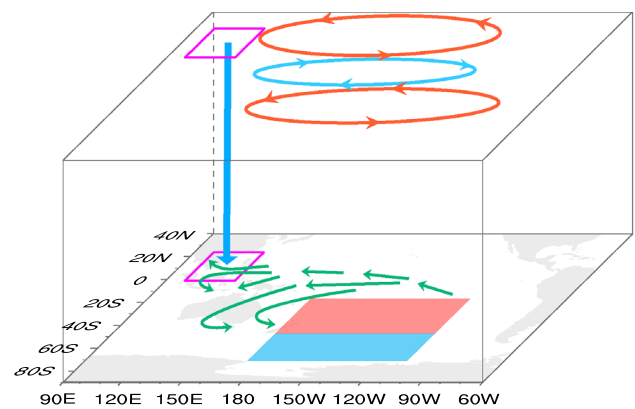

Fig. 11 Schematic diagram describing the influence of the May SAM related SPD (*blue and red box*) on the SCSSM. The *green arrows* indicate the JJAS anomalous circulation related with JJAS SPD. The *blue arrow* indicates the JJAS anomalous descending motion related with JJAS SPD. The *red and blue ellipse* indicate the SNP teleconnection pattern. The *magenta box* marks the SCS monsoon region (0–25°N, 100–125°E)

new teleconnection phenomenon deserves further attention. Launching out the further research into the SNP teleconnection, could contribute to an improved understanding of the possible physical mechanisms underlying in the connection between the SH high-latitude and NH climate variability. In particular, the following aspects require attention: the space–time evolution and formation mechanism of the SNP; the multi-scale variation characteristics and related dynamics of the SNP; the impact of the multi-scale variation of the SNP on weather and climate and possible physical mechanisms; the predictability of the multi-scale SNP and corresponding forecast theories and methods; the future tendency of the SNP under global warming scenarios, and so on.

References

An ZS, Wu GX, Li JP, Sun YB, Liu YM, Zhou WJ, Cai YJ, Duan AM, Li L, Mao JY, Cheng H, Shi ZG, Tan LC, Yan H, Ao H, Chang H, Feng J (2015) Global monsoon dynamics and climate change. Annu Rev Earth Planet Sci 43:29–77

Berrisford P, Kallberg P, Kobayashi S et al (2011) The ERA-Interim archive version 2.0. Eur Cent Medium Range Weather Forecasts ERA Tech Rep 1:23

Chen LX, Zhang B, Zhang Y (2006) Progress in research on the East Asian Monsoon. J Appl Meterol Sci 17:711–724

Chen G, Plumb RA, Lu J (2010) Sensitivities of zonal mean atmospheric circulation to SST warming in an aqua-planet model. Geophys Res Lett 37:L12701

Ding YH (1992) Summer monsoon rainfalls in China. J Meteorol Soc Jpn 70:373–396

Ding YH, Li CY, He JH, Chen LX, Gan ZJ, Qian YF, Yan JY, Wang DX, Shi P, Wan WD, Xu JP, Li L (2004) South China Sea monsoon experiment (SCSMEX) and the East Asian monsoon (in chinese). Acta Meteorol Sin 62:561–586

Ding QH, Steig EJ, Battisti DS, Wallace JM (2012) Influence of the tropics on the southern annular mode. J Clim 25:6330–6348

Ding RQ, Li JP, Tseng YH (2015) The impact of South Pacific extratropical forcing on ENSO and comparisons with the North Pacific. Clim Dyn 44:2017–2034

Dou J, Wu ZW, Zhou YF (2016) Potential impact of the May Southern Hemisphere annular mode on the Indian summer monsoon rainfall. Clim Dyn. doi:10.1007/s00382-016-3380-4

Feng J, Li JP (2009) Variation of the South China Sea summer monsoon and its association with the global atmosphere circulation and sea surface temperature. Chin J Atmos Sci 33:568–580 **(in Chinese)**

Feng J, Li JP, Li Y, Zhu JL, Xie F (2015) Relationships among the monsoon-like southwest Australian circulation, the southern annular mode, and winter rainfall over southwest Western Australia. Adv Atmos Sci 32:1063–1076

Fogt R, Jones JM, Renwick J (2012) Seasonal zonal asymmetries in the Southern annular mode and their impact on regional temperature anomalies. J Clim 25:6253–6270

Frierson DM, Lu J, Chen G (2007) Width of the Hadley cell in simple and comprehensive general circulation models. Geophys Res Lett 34:L18804

Fukutomi Y, Yasunari T (2002) Tropical-extratropical interaction associated with the 10–25-day oscillation over the western Pacific during the Northern summer. J Meteorol Soc Jpn 80:311–331

Gillett NP, Kell T, Jones P (2006) Regional climate impacts of the Southern annular mode. Geophys Res Lett 33:L23704

Gong DY, Wang SW (1998) Antarctic oscillation: concept and applications. Chin Sci Bull 43:734–738

Hartmann DL, Lo F (1998) Wave-driven zonal flow vacillation in the Southern Hemisphere. J Atmos Sci 55:1303–1315

Hoskins BJ, Karoly DJ (1981) The steady linear response of a spherical atmosphere to thermal and orographic forcing. J Atmos Sci 38:1179–1196

Huang G (2004) An index measuring the interannual variation of the East Asian summer monsoon-the EAP index. Adv Atmos Sci 21:41–52

Huang RH, Li WJ (1987) Influence of heat source anomaly over the tropical western Pacific on the subtropical high over East Asia. In: Proceedings International Conference on the General Circulation of East Asia, Chengdu, China, April 10–15, 1987, pp 40–45

Huang RH, Li WJ (1988) Influence of heat source anomaly over the western tropical Pacific on the subtropical high over East Asia and its physical mechanism. Chin J Atmos Sci (in Chinese) 12(s1):107–116

Kalnay E et al (1996) The NCEP/NCAR 40-year reanalysis project. Bull Am Meteorol Soc 77:437–471

Kawamura R, Murakami T, Wang B (1996) Tropical and mid-latitude 45-day perturbations over the Western Pacific during the northern summer. J Meteorol Soc Jpn 74:867–890

Lau KM, Yang S (1997) Climatology and Interannual variability of the Southeast Asian summer monsoon. Adv Atmos Sci 14:141–162

Lestari RK (2010) Mechanisms of seasonal march of precipitation over Maritime Continent Regions: observational and model studies. VDM Publishing House, Germany

Li JP (2016) Impacts of annular modes on extreme climate events over the East Asian monsoon region. In: Li JP (ed) Dynamics and predictability of large-scale, high-impact weather and climate events. Cambridge University Press, UK

Li JP, Hu DX (2011) Preface. In: Li JP, Wu GX, Hu DX (eds) Ocean–atmosphere interaction over the joining area of Asia Indian-Pacific ocean and its impact on the short-term climate variation in China (in Chinese). China Meteorological Press, Beijing, pp 8–12

Li YJ, Li JP (2012) Propagation of planetary waves in the horizontal non-uniform basic flow (in Chinese). Chin J Geophys 55:361–371

Li JP, Wang JX (2003) A modified zonal index and its physical sense. Geophys Res Lett 30:1632

Li JP, Zeng QC (2000) Significance of the normalized seasonality of wind field and its rationality for characterizing the monsoon. Sci Chin 43:647–653

Li JP, Zeng QC (2002) A unified monsoon index. Geophys Res Lett 29:1274

Li JP, Zeng QC (2003) A new monsoon index and the geographical distribution of the global monsoons. Adv Atmos Sci 20:299–302

Li JP, Zeng QC (2005) A new monsoon index, its interannual variability and relation with monsoon precipitation. Clim Environ Res 10:351–365

Li CY Zhang LP (1999) Summer monsoon activities in the South China sea and its impacts. Chinese J Atmos Sci (in Chinese) 23(3):257–266

Li JP, Wu ZW, Jiang ZH, He JH (2010) Can global warming strengthen the East Asian summer monsoon? J Clim 23:6696–6705

Li JP, Ren RC, Qi YQ, Wang FM, Lu RY, Zhang PQ, Jiang ZH, Duan WS, Yu F, Yang YZ (2013a) Progress in air-land-sea interaction in Asian and their role in global and Asian climate change. Chin J Atmos Sci (in Chinese) 37:518–538

Li JP, Sun C, Jin FF (2013b) NAO implicated as a predictor of Northern Hemisphere mean temperature multidecadal variability. Geophys Res Lett 40(20):5497–5502

Li YJ, Li JP, Feng J (2013c) Boreal summer convection oscillation over the Indo-Western Pacific and its relationship with the East Asian summer monsoon. Atmos Sci Lett 14:66–71

Li YJ, Li JP, Jin FF, Zhao S (2015) Interhemispheric propagation of stationary Rossby waves in a horizontally nonuniform background flow. J Atmos Sci 72:3233–3256

Limpasuvan V, Hartmann DL (1999) Eddies and the annular modes of climate variability. Geophys Res Lett 26:3133–3136

Limpasuvan V, Hartmann DL (2000) Wave-maintained annular modes of climate variability. J Clim 13:4414–4429

Lin AL, Gu DJ, Zheng B, Li CH, Ji ZP (2013) Relationship betwwen South China Sea summer monsoon onset and Southern Ocean sea surface temperature variation. Chin J Geophys (in Chinese) 56:383–391

Liu T, Li JP, Zheng F (2015) Influence of the Boreal autumn SAM on winter precipitation over land in the Northern Hemisphere. J Clim 28:8825–8839

Liu T, Li JP, Feng J, Wang XF, Li Y (2016) Cross-seasonal relationship between the Boreal autumn SAM and winter precipitation in the Northern Hemisphere in CMIP5. J Clim 29:6617–6636

Lorenz DJ, Hartmann DL (2001) Eddy-zonal flow feedback in the Southern Hemisphere. J Atmos Sci 58:3312–3327

Marshall GJ (2003) Trends in the Southern annular mode from observations and reanalyses. J Clim 16:4134–4143

Marshall GJ, Connolley WM (2006) Effect of changing Southern Hemisphere winter sea surface temperatures on Southern annular mode strength. Geophys Res Lett 33:L17717

Murakami T, Matsumoto J (1994) Summer monsoon over the Asian continent and western north Pacific. J Meteorol Soc Jpn 72:719–745

Murakami T, Chen LX, Xie A (1986) Relationship among seasonal cycles, low-frequency oscillations, and transient disturbances as revealed from outgoing longwave radiation data. Mon Weather Rev 114:1456–1465

Nan SL, Li JP (2003) The relationship between the summer precipitation in the Yangtze River valley and the boreal spring Southern Hemisphere annular mode. Geophys Res Lett 30:2266

Nan SL, Li JP (2005a) The relationship between the summer precipitation in the Yangtze River valley and the boreal spring Southern Hemisphere annular mode: I. Basic facts (in Chinese). Acta Meteorol Sin 63:837–846

Nan SL, Li JP (2005b) The relationship between the summer precipitation in the Yangtze River valley and the boreal spring Southern Hemisphere annular mode: II. The role of the Indian Ocean and South China Sea as an ''oceanic bridge'' (in Chinese). Acta Meteorol Sin 63:847–856

Nan SL, Li JP, Yuan XJ, Zhao P (2009) Boreal spring Southern Hemisphere annular mode, Indian Ocean sea surface temperature, and East Asian summer monsoon. J Geophys Res 114:D02103

Nitta TS (1987) Convective activities in the tropical western Pacific and their impact on the Northern Hemisphere summer circulation. J Meteorol Soc Jpn 64:373–390

Prabhu A, Kripalani RH, Preethi B, Pandithurai G (2015) Potential role of the February–March Southern annular mode on the Indian summer monsoon rainfall: a new perspective. Clim Dyn 47:1161–1179

Rayner NA, Parker DE, Horton EB, Folland CK, Alexander LV, Rowell DP (2003) Global analyses of sea surface temperature, sea ice, and night marine air temperature since the late nineteenth century. J Geophys Res 108:4407

Saurral RI, Doblas-Reyes FJ, García-Serrano J (2017) Observed modes of sea surface temperature variability in the South Pacific region. Clim Dyn. doi:10.1007/s00382-017-3666-1

Shi F, Li JP, Wilson RJS (2014) A tree-ring reconstruction of the South Asian summer monsoon index over the past millennium. Sci Rep 4:6739

Smith TM, Reynolds RW, Peterson TC, Lawrimore J (2008) Improvements to NOAA's historical merged land-ocean surface temperature analysis (1880–2006). J Clim 21:2283–2296

Sun JQ (2010) Possible impact of the boreal spring Antarctic Oscillation on the North American summer monsoon. Atmos Ocean Sci Lett 3:232–236

Sun JQ, Wang HJ, Yuan W (2010) Linkage of the boreal spring Antarctic Oscillation to the West African summer monsoon. J Meteorol Soc Jpn 88:15–28

Sun C, Li JP, Zhao S (2015) Remote influence of Atlantic multidecadal variability on Siberian warm season precipitation. Sci Rep. doi:10.1038/srep16853

Sun C, Li JP, Ding R Q, Jin Z (2016) Cold season Africa–Asia multidecadal teleconnection pattern and its relation to the Atlantic multidecadal variability. Clim Dyn. doi:10.1007/s00382-016-3309-y

Tao SY, Chen LX (1987) A review of recent research on the East Asian summer monsoon in China. Monsoon meteorology. Oxford University Press, Oxford

Terray P (2011) Southern Hemisphere extra-tropical forcing: a new paradigm for El Niño-Southern Oscillation. Clim Dyn 36:2171–2199

Thompson DWJ, Solomon S (2002) Interpretation of recent Southern Hemisphere climate change. Science 296:895–899

Thompson DWJ, Wallace JM (2000) Annular modes in the extratropical circulation. Part I: month-to-month variability. J Clim 13:1000–1016

Viswambharan N, Mohanakumar K (2012) Signature of a southern hemisphere extratropical influence on the summer monsoon over India. Clim Dyn 41:367–379

Wang B, Huang F, Wu ZW, Yang J, Fu X, Kikuchi K (2009) Multiscale climate variability of the South China Sea monsoon: a review. Dyn Atmos Oceans 47:15–37

Wu RG, Wang B (2000) Interannual variability of summer monsoon onset over the western North Pacific and the underlying processes. J Clim 13:2483–2501

Wu RG, Wang B (2001) Multi-stage onset of the summer monsoon over the western North Pacific. Clim Dyn 17:277–289

Wu ZW, Li JP, Wang B, Liu X (2009) Can the Southern Hemisphere annular mode affect China winter monsoon? J Geophys Res 114:D11107

Wu ZW, Dou J, Lin H (2015) Potential influence of the November–December Southern Hemisphere annular mode on the East Asian winter precipitation: a new mechanism. Clim Dyn 44:1215–1226

Wu ZW, LI XX, Li YJ, Li Y (2016) Potential influence of Arctic sea ice to the interannual variations of East Asian spring precipitation. doi:10.1175/JCLI-D-15-0128.1

Xu HL, Li JP, Feng J, Mao JY (2013) The asymmetric relationship bewteen the winter NAO and the precipitation in southwest China. Acta Meteorol Sin 70:1276–1291

Zhao S, Li JP, Li YJ (2015) Dynamics of an interhemispheric teleconnection across the critical latitude through a southerly duct during boreal winter. J Clim 28:7437–7456

Zheng F, Li JP (2012) Impact of preceding boreal winter Southern Hemisphere annular mode on spring precipitation over south China and related mechanism (in Chinese). Chin J Geophys 55:3542–3557

Zheng F, Li JP, Liu T (2014a) Some advances in studies of the climatic impacts of the Southern Hemisphere annular mode. J Meteorol Res 28:820–835

Zheng J Y, Li JP, Feng J (2014b) A dipole pattern in the Indian and Pacific oceans and its relationship with the East Asian summer monsoon. Environ Res Lett 9:074006

Zheng F, Li JP, Wang L, Xie F, Li XF (2015a) Cross-seasonal influence of the December–February Southern Hemisphere annular mode on March–May meridional circulation and precipitation. J Clim 28:6859–6881

Zheng F, Li JP, Feng J, Li YJ, Li Y (2015b) Relative importance of the Austral Summer and Autumn SAM in modulating Southern Hemisphere extratropical autumn SST. J Clim 28:8003–8020

Zheng F, Li JP, Li YJ, Zhao S, Deng DF (2016) Influence of the Summer NAO on the Spring-NAO-Based Predictability of the East Asian Summer Monsoon. J Appl Meteorol Clim. doi:10.1175/JAMC-D-15-0199.1

Zhu CW, Nakazawa T, Li JP (2003) The 30–60 day intraseasonal oscillation over the Western North Pacific Ocean and its impacts on summer flooding in China during 1998. Geophys Res Lett 30:GL017817

Zhu JL, Liao H, Li JP (2012) Increases in aerosol concentrations over eastern China due to the decadal-scale weakening of the East Asian summer monsoon. Geophys Res Lett 39:L09809